Ionic Liquid Treatment for Efficient Sample Preparation of Hydrated Bone for Scanning Electron Microscopy

Liza-Anastasia DiCecco[1], Andrew D'Elia[1], Cheryl Quenneville[2,3], Leyla Soleymani[2,4], Kathryn Grandfield[1,2*]

[1] Department of Materials Science and Engineering, McMaster University, Hamilton, ON, Canada

[2] School of Biomedical Engineering, McMaster University, Hamilton, ON, Canada

[3] Department of Mechanical Engineering, McMaster University, Hamilton, ON, Canada

[4] Department of Engineering Physics, McMaster University, Hamilton, ON, Canada

[*] Corresponding author:
Prof. Kathryn Grandfield
McMaster University
1280 Main Street West
Hamilton, ON, L8S 4L7
Canada
Email: kgrandfield@mcmaster.ca

Abstract

This study presents a new protocol for preparing bone samples for scanning electron microscopy (SEM) using a room temperature ionic liquid (RTIL) treatment method. RTIL-based solutions can be adopted as an alternative to lengthy and laborious traditional means of preparation for SEM due to their unique low-vapour pressure and conductive properties. Applied to biological samples, RTILs can be used quickly and efficiently to observe hydrated, unfixed structures in typical SEM systems. This first-time feasibility study of the optimization of this protocol for bone was explored through various SEM modalities using two distinct ionic liquids, 1-ethyl-3-methylimidazolium tetrafluoroborate ([EMI][BF_4]) and 1-butyl-3-methyl imidazolium tetrafluoroborate ([BMI][BF_4]), at varying concentrations of 5, 10, and 25% v/v in aqueous solution through an addition-based method. Based on qualitative observations in the SEM, a 60-second solution addition treatment of 10% v/v [BMI][BF_4] performed the best in imaging hydrated, unfixed bone samples, resulting in minimal charge buildup and no solution pooling on the surface. The treatment was applied effectively to a variety of bone samples, notably flat and polished, as well as highly topographical bone fracture surfaces of both healthy and osteoporotic human bone samples. In comparison to conventionally dehydrated bone, the RTIL treatment better preserved the natural bone structure, resulting in minimal microcracking in observed structures.

Graphical Abstract

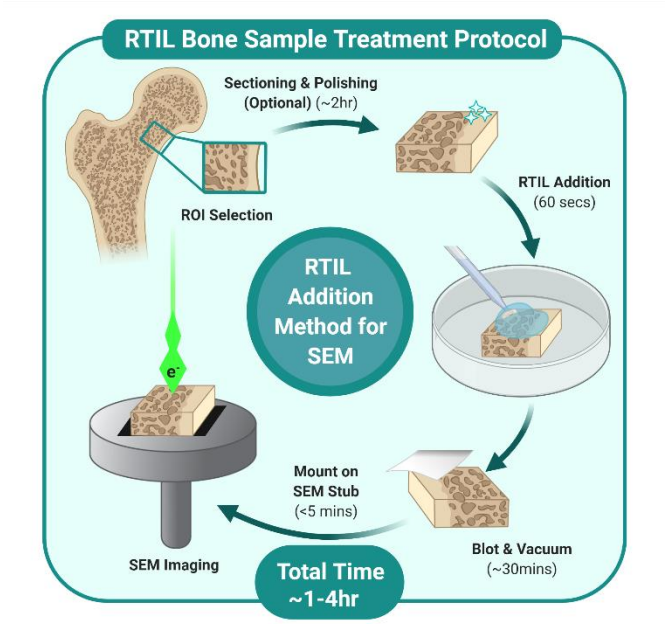

Keywords:

Bone, ionic liquids, mineralization, biological imaging, scanning electron microscopy

Research Highlights:

1) New protocol to prepare bone for scanning electron microscopy using ionic liquids
2) Improvement in bone sample fidelity vs traditional preparation methods
3) Observed unfixed hydrated bone without preparation artifacts

1. Introduction

In biological imaging communities, bone has been a topic of high interest in scanning electron microscopy (SEM) for well over half a century (Shah et al., 2019). The study of bone's complex hierarchical structure using SEM can elicit key details on bone sample health (Milovanovic et al., 2018), disease mechanisms (Dempster et al., 1986), failure mechanisms (Braidotti et al., 2000; Hiller et al., 2003), bone ingrowth behaviour for orthopedic implant applications (Shah et al., 2016), and much more. However, due to restrictions on the high vacuum state of typical SEM systems, conventional preparation methods typically including fixation, dehydration and conductive coating, are required to make structural observations on bone features. While these methods aid in preserving bone structure for long-term study, they also risk altering the natural morphologies present in these tissues (Kellenberger et al., 1992; Li et al., 2017; McKee et al., 1991; Utku et al., 2008). Moreover, bone is a non-conductive material, which presents other challenges for SEM imaging, such as charging.

As such, researchers are exploring alternative methods of sample preparation to observe biological materials in their natural hydrated states through SEM. Recently, the use of room temperature ionic liquids (RTILs) has risen in popularity as a sample treatment method for this purpose. RTILs are ionic salts that exist in the liquid state at room temperature, composed of ions and short-lived ionic pairs (Welton, 1999). Apart from their liquid nature, two particularly important aspects of RTILs include their high conductivity and low vapour pressure (Hagiwara and Ito, 2000), which make them highly applicable in SEM. This allows for samples to be treated by RTILs and be imaged in their natural hydrated, unfixed state. Kuwabata et al. were the first to show that RTILs can be observed in high vacuum SEM and experience limited charge buildup during observation (Kuwabata et al., 2006). A wide range of biological samples have been observed following similar treatments since (Golding et al., 2016; Komai et al., 2014; Lee et al., 2021; Lu et al., 2019; Tsuda et al., 2011). Notably, hydrophilic RTILs have been shown in several instances to be more effective in imaging hydrated biological samples in comparison to hydrophobic RTILs (Arimoto et al., 2008; Ishigaki et al., 2011a).

An RTIL-based preparation technique can be used as a facile, relatively inexpensive treatment option for biological samples in lieu of time-consuming traditional sample preparation methods required for typical SEM configurations. For bone samples, conventional SEM preparation methods can be lengthy and laborious (Binkley et al., 2020; Tedesco et al., 2017). Figures 1 and 2 can be used for comparing the proposed RTIL treatment pathway for bone to traditional preparation methodologies for SEM observation. In conventional methodologies, fixation and dehydration steps can take upwards of 40 hours per sample. Considering equipment availability and lab working hours, it can take weeks to fully prepare a bone sample for SEM observation. This is not considering embedding in resin and staining processes – which can increase the time required for sample preparation (Chissoe et al., 1995; Reznikov et al., 2013). In contrast, RTIL treatments can be employed to observe bone within hours, allowing for quicker sample turn-around time and improved productivity. Two distinct RTIL treatment methods can be identified in literature: 1) immersion, where samples are immersed in solution, and 2) addition, where the RTIL solution is added directly to samples and potentially drained via membrane filtering (DiCecco et al., 2021). In general, the immersion method is more effective for large biological samples while an addition-based method is preferred for smaller specimens (Tsuda and Kuwabata, 2020). RTIL treatment exposure times may vary to allow for sufficient penetration of the sample and is often dependent on sample size, the type of biological sample, and the solution used (Tsuda et al., 2011), though generally, this treatment is less than 10 minutes (DiCecco et al., 2021; Tsuda and Kuwabata, 2020).

Limited works have explored this technique to study mineralized tissues, and—to our knowledge—none have used this technique to observe human bone. In works produced by Abe et al., RTIL treatment is shown to be effective for SEM observation of mineralized, hard tissue shellfish samples, achieving a similar resolution to images produced using Pt/Pd sputtering techniques (Abe et al., 2012). This work also highlighted the capacity of RTILs to be used in conjunction with elemental analyses, such as energy-dispersed fluorescent X-ray spectroscopy (EDS) (Abe et al., 2012). The successful utilization of RTIL-based SEM preparation protocols applied to stiff, porous wooden structures to study their natural composite hierarchical structure and topographical features (Kanbayashi and Miyafuji, 2016; Lu et al., 2019) provides insight on the potential of these techniques in studying bone – a similarly organic, porous composite material with complex hierarchical features (Binkley and Grandfield, 2017). This suggests that similarly-

adopted RTIL treatments can be used to investigate hydrated, unfixed bone structures with polished or highly topographical surfaces in SEM.

Herein, we investigated RTIL sample preparation methodologies and SEM imaging conditions for hydrated bone tissues using two different RTILs at various concentrations. This first-of-its-kind work presents a simple and effective protocol to image hydrated, unfixed bone samples in the SEM and with EDS analysis capabilities. The study focuses on bone from the femoral neck as a clinically relevant region of interest, where applications of this proposed protocol are highlighted for healthy cortical and trabecular bone, as well as for flat and topographical fracture surfaces of diseased tissue, such as osteoporotic bone. This work bridges the gap between bone research and RTIL-methods developed in chemistry, showing the potential of using this novel non-conventional SEM preparation method for the analysis of mineralized bone tissue.

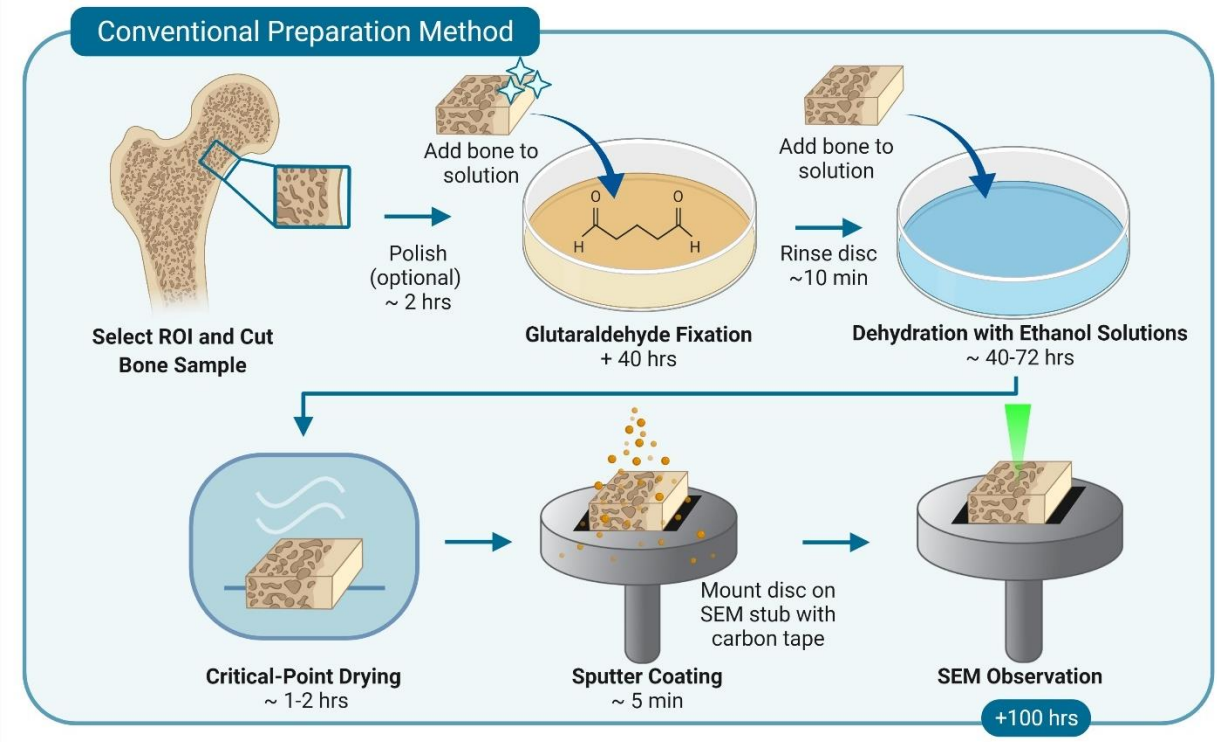

Figure 1. Illustration of conventional SEM preparation methods used for bone with time of each step approximated (estimation for bone specimens 1 cm^3 or larger). Note that staining and embedding procedures would further lengthen the preparation time.

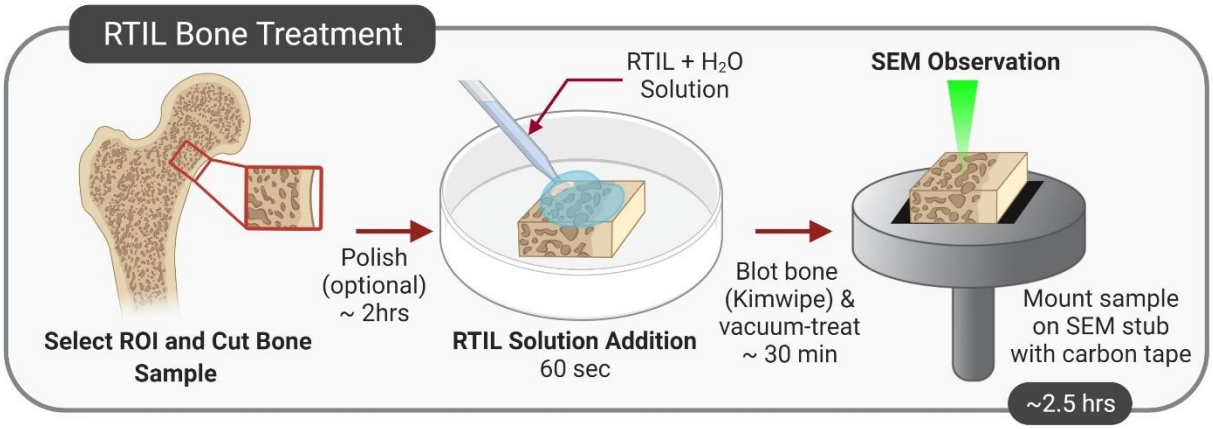

Figure 2. Schematic illustrating the specific RTIL treatment process used in this work for SEM imaging of hydrated, unfixed bone samples.

2. Materials and Methods

2.1. Bone Preparation

This research and sample acquisition was approved by the Hamilton Integrated Research Ethics Board (HiREB 2015-0990-T). Bone sections were procured from the proximal femur, at the femoral neck, of three fresh-frozen human cadaveric femurs (Table 1), which were cleaned of all exterior soft tissue. Each sample had an associated T-score, a common clinical measure of osteoporosis determined by dual energy x-ray absorptiometry x-ray (DEXA) imaging, where scores below -2.5 indicate osteoporosis, scores between -1.0 and -2.5 are considered osteopenic, and scores above -1.0 are indicative of healthy bone. Samples from the femoral neck of a healthy bone specimen featuring both trabecular and cortical sections were used to optimize the RTIL protocol. This protocol was then adopted for the investigation of unfractured and fractured osteoporotic bone.

To prepare bone for this study, large bone sections were cut at the base of the femoral neck with a handsaw, perpendicular to the neck axis at the inferior aspect. The bone was further sectioned into smaller pieces using a water-cooled, diamond-edged precision low-speed saw (Buehler, Illinois, USA). Specimens were kept frozen at -21°C and were thawed for a minimum of twelve hours prior to sectioning. Samples were hand-ground and polished using an incremental grit scheme with 400, 800, 1200, and 2400 grit emery paper and a final 0.5 μm diamond suspension on a polishing pad (Buehler, Illinois, USA). All samples were treated with the same preparation scheme, apart from the fractured bone samples which were not ground and polished. The resulting samples were approximately 1 cm × 1 cm × 0.5 cm in size, containing both cortical and trabecular bone structures.

As a control, healthy bone samples were also prepared using conventional methods, where samples were subjected to the same polishing scheme and subsequently dehydrated through a graded series of ethanol in aqueous solution (50, 70, 70, 90, 90, 100, 100%) for six hours at each stage. Samples were ultrasonically cleaned in pure ethanol, air dried, and sputter-coated with 10 nm gold using a Precision Etching Coating System (PECS II) coater (Gatan Inc., CA, USA) before observation.

Table 1. Summary of human bone specimen information imaged in this study.

Bone Description & Type	Anatomical Location	Sex	Age	Total T-Score	Neck T-Score
Healthy femur	Femoral neck, intact site (superior half cross-section)	F	70	-1.0	-1.1
Osteoporotic femur	Femoral neck, intact site (interior half cross-section)	F	99	-2.6	-3.2
Osteoporotic femur, fractured in the study featured in ref. (Jazinizadeh et al., 2020)	Femoral neck, fracture site (superior half cross-section)	F	76	-3.0	-4.6

2.2. RTIL Application Methods

Prior to RTIL treatment, prepared bone samples were ultrasonically cleaned in ultra-pure Milli-Q water. The two hydrophilic RTILs investigated were 1-ethyl-3-methylimidazolium tetrafluoroborate and 1-butyl-3-methyl imidazolium tetrafluoroborate (Sigma-Aldrich Canada Co, Oakville, CA) referred to as [EMI][BF_4] and [BMI][BF_4], respectively. The treatment considered for these samples was an addition-based method (Figure 2) where varying concentrations of 5, 10, & 25% v/v RTIL in ultra-pure Milli-Q water was applied to samples [19, 20]. In detail, solutions were prepared with the appropriate concentration and heated by submerging in a 40 °C water bath before application to bone to reduce the viscosity and improve their ability to spread onto samples. For treatment, 100 μl of RTIL solution was pipetted onto bone samples for a 60 second exposure time, after which excess solution was gently blotted away using precision wipes (Kimwipes). Samples were then mounted onto standard 12.7 mm diameter sized

aluminum SEM stubs with double-sided carbon tape and aluminum tape. Before imaging, samples were placed in a desiccator under vacuum for 30 minutes to further eliminate excess liquid.

2.3. SEM Imaging

Bone samples were imaged using a tungsten filament equipped JEOL 6610LV SEM (JEOL, Tokyo, Japan) SEM and backscattered electron (BSE) images were acquired. Microscope parameters including accelerating voltage and vacuum modes were optimized for best imaging results. An electron beam accelerating voltage of 15kV was found to be optimal for imaging, where limited charging and no visible electron-burning of the tissue were experienced. Both low-vacuum imaging at 30 Pa and conventional high-vacuum mode ranging from 10^{-4} – 10^{-5} Pa in session were investigated, with a consistent working distance of 10 mm. Elemental maps were collected by EDS with an Oxford Instruments X-Max 20 mm^2 area Silicon Drift EDS Detector (SDD) (Oxford Instruments, Oxford, UK) at 15kV. EDS was performed in low-vacuum mode post-calibration using pure silicon and aluminum specimens as standards. EDS maps were analyzed and exported using the Oxford Instruments AZtec 3.3 software. Images were assessed and compared on a qualitative basis, where factors such as charging, liquid pooling, spatial resolution, and ease of imaging were considered together in identifying an ideal treatment.

3. Results and Discussion

3.1. Effect of RTIL Selection and Concentration

Despite the low conductivity of bone tissue, little to no charging artifacts were observed following RTIL treatment in images acquired at a relatively high acceleration voltage of 15 kV, suggesting that RTILs impart adequate conductivity to the sample surface. Images of healthy bone taken in low vacuum mode are shown in Fig. 3 to demonstrate the effectiveness of the two RTILs at concentrations of 5, 10 and 25% v/v. Throughout the RTIL optimization process, the 10% v/v [BMI][BF_4] treatment had the best performance overall during SEM imaging when considering the mitigation of liquid pooling (Fig. S1) and charging effects (Fig. S2) as well as qualitative imaging quality in both high and low vacuum schemes.

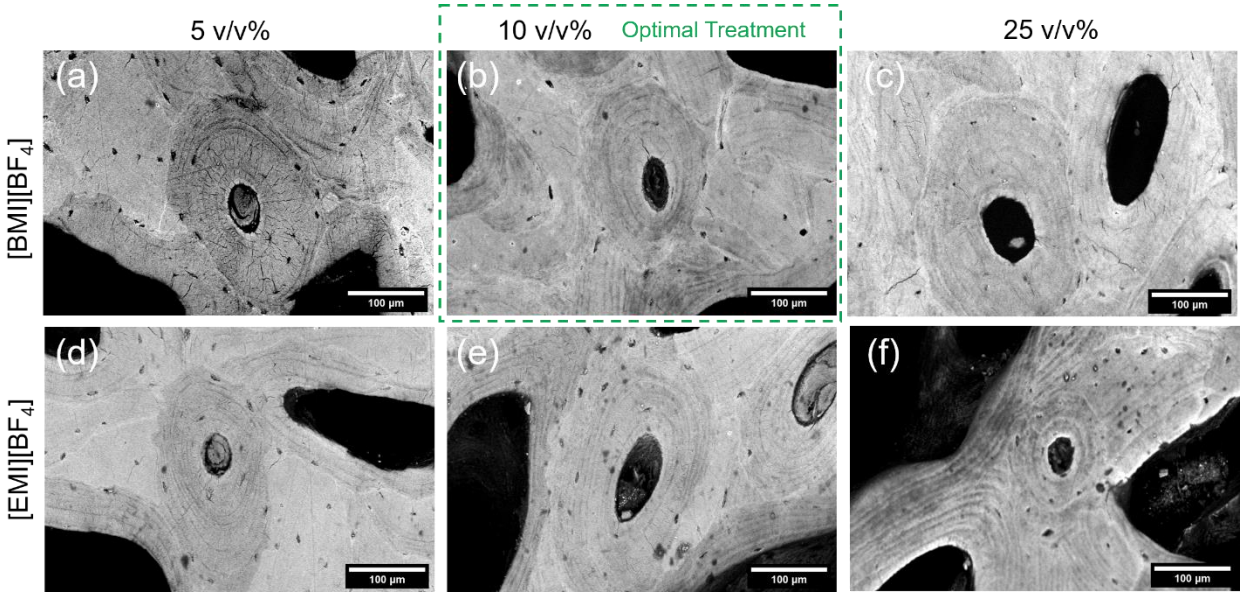

Figure 3. BSE SEM images of healthy bone taken in low-vacuum conditions. Samples were treated with 5, 10, or 25% v/v of [BMI][BF_4] (a-c) or [EMI][BF_4] (d-f) in water for 60 s. All images show osteons in a central location of each image surrounded by concentric lamellae bone centralized around a harversian canal. At higher concentrations of 25% v/v, fine details in the bone structure were obscured while liquid pooling was also observed on the structure. The 10% v/v had limited issues with charging and could be used readily for high resolution in both low and high-vacuum conditions, thus performed optimally within the treatments explored.

At concentrations of 25% v/v, both RTIL treatments showed signs of liquid pooling on the sample surface, which resulted in a loss of resolution, and, in secondary electron (SE) mode, the appearance of liquid pooling artifacts (Fig. S1). RTIL solution pooling on a sample surface can greatly impact the quality of SEM imaging, especially when observing highly topographical samples in SE mode. This can lead to the loss of sharp and/or fine morphological features and potentially hide topographical features from being detected. Pooling typically occurs when using concentrated RTILs due to their viscous nature (Arimoto et al., 2008; Yanaga et al., 2012).

Although pooling was observed infrequently during imaging, it was found that BSE mode could still be used to observe these regions. The depth of the BSE signal likely allowed for key features to be resolved, despite the liquid layer, permitting the observation of underlying bone structures. Thus, within certain thicknesses, liquid pooling has minimal influence on the resolution of bone features in BSE mode due to the depth of signal origin; however, excess pooling can obscure features and lead to poor quality SEM images (Fig. S1).

Samples treated with 5% v/v [EMI][BF_4] exhibited some charging effects, resulting in notable imaging artifacts such as noise and distortions from scanning (Fig, S2). Similar artifacts were noted for the 5% v/v [BMI][BF_4] and 10% v/v [EMI][BF_4] treatments in high vacuum trials, particularly on trabecular bone segments. In other works, similar charging trends are noted for biological samples imaged at lower RTIL concentrations, where excess surface charging has been found when below-optimal concentrations due to insufficient conductivity (Ishida et al., 2016; Yanaga et al., 2012). For both RTILs, the 10% v/v treatment performed well in high and low vacuum and had mitigated pooling and charging effects; however, the [EMI][BF_4] scheme was observed to leave contaminants in isolated regions of the sample surface. Therefore, overall, treatment with [BMI][BF_4] resulted in universally higher quality SEM images than those imaged using [EMI][BF_4] and thus the 10% v/v [BMI][BF_4] was found the most optimal in the testing schemes considered. While commercially purchased high purity [EMI][BF_4] (=>99%) was used in the unpurified state herein, further purification means could help mitigate contaminants and to yield improved imaging results (Tsuda et al., 2011; Tsuda and Kuwabata, 2020).

3.2. RTILS for Imaging Cortical Bone and Trabecular Bone

With all treatment schemes, osteons in cortical bone can be clearly identified at the centre of each image in Fig. 3 as circular features composed of concentric layers of lamellae bone centralized around a haversian canal that contains blood vessels (Kini and Nandeesh, 2012). Lacunae, the sites housing bone cells called osteocytes, appear as blacker contrast smaller ellipsoidal shapes and can be resolved within the osteonal layers as well as the interstitial bone at all RTIL concentrations. Conventionally, the advantage of BSE SEM of bone is to distinguish regions of varying mineral content qualitatively or quantitatively by greyscale intensity (Roschger et al., 1998). In cortical bone, variations in mineral density can be readily observed between osteons and interstitial bone surrounding osteons. Interstitial bone, which is generally the oldest least remodelled bone tissue, tends to have higher mineralization densities and thus appears brighter in BSE mode in comparison to remodelled newer osteons, which typically have lower mineral amounts and appear darker (Milovanovic et al., 2018; Shah et al., 2019; Skedros et al., 2005). This is particularly evident in the central osteons features in Fig 3. – all representing nearly fully circular, and therefore secondary, osteons created during bone remodelling (Kini and Nandeesh, 2012).

Figure 4 highlights higher magnification images of both cortical and trabecular bone that could be achieved using the 10% v/v [BMI][BF_4] treatment in low vacuum, where a haversian canal in cortical bone is shown in Fig. 4 (a,b) while trabecular bone is featured in Fig. 4 (c,d). Lacunae osteocyte networks can be observed in the bone structures of the samples in Fig. 4 (b) and (d), while finer micro-scale features of the bone can be resolved. Considering trabecular segments, charging artifacts can be challenging to mitigate in un-embedded trabecular bone segments even using conventional preparation methods. The higher porosity of trabecular bone results in free-floating unmounted bone fragments that interfere with the beam and subsequently create imaging challenges due to difficulty establishing a conductive path to ground the incoming electron beam in un-embedded samples (Boyde et al., 1986; Boyde and Jones, 1996). However, they were effectively observed using the 10% v/v [BMI][BF_4] treatment (Fig. 4 (c,d)), where lamellar hemi-osteons and lacunae where osteocytes reside can clearly be distinguished.

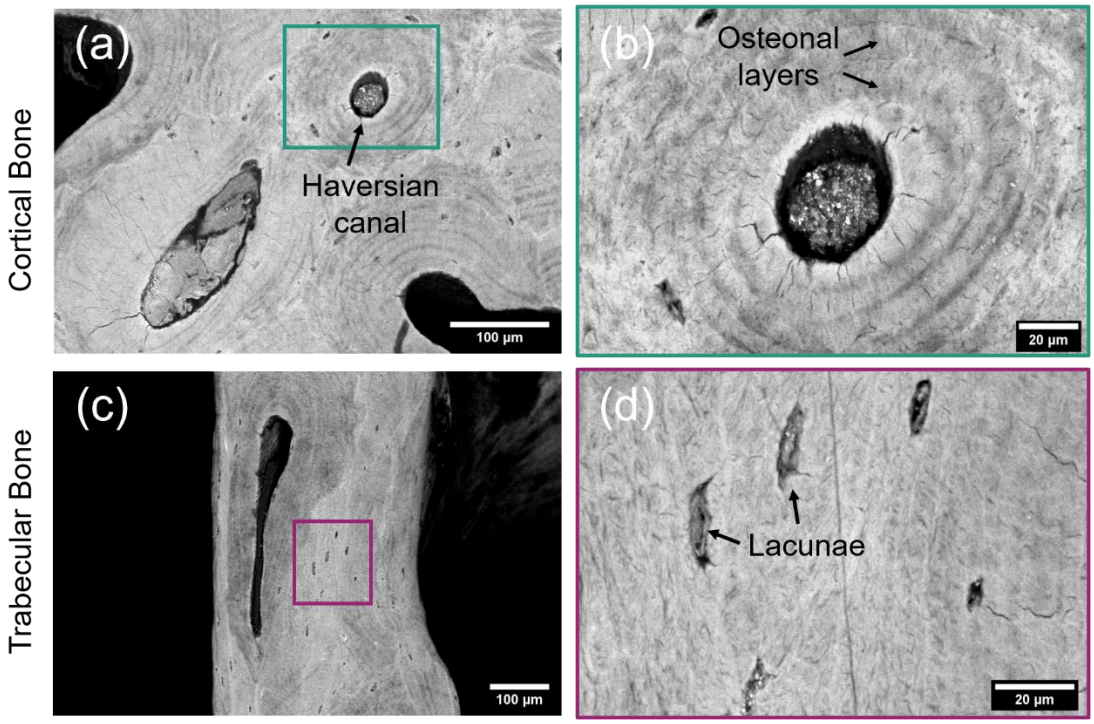

Figure 4. BSE SEM images of healthy bone in low-vacuum conditions treated with 10% v/v [BMI][BF_4]. Both cortical bone (a,b) with visible harversian canals and trabecular bone (c,d) were easily imaged with this concentration. At higher magnification (b,d) both osteonal and lamellar bone as well as lacunae where osteocytes are located are visible. Minimal cracks are observed.

3.3. Application to Osteoporotic Bone

The application of 10% v/v [BMI][BF4] can readily be used to observe a variety of healthy or pathological bone tissues in both low and high vacuum SEM conditions. Figures 5 and 6 highlight the high vacuum imaging capabilities in secondary electron (SE) and BSE modes of this method, showing that RTILs facilitate imaging of both polished (Fig. 5) and fractured (Fig. 6) osteoporotic bone. The imaging illustrates that the optimized RTIL treatment can be used to i) observe samples in high vacuum modes, ii) study fractured or highly topographical bone specimens, & iii) efficiently and quickly observe diseased bone such as osteoporotic bone in SEM.

Figure 5 shows high-resolution images of an osteon in osteoporotic cortical bone. Osteonal lamellae can be easily observed, measured, and counted using images captured from this preparation technique. This helps show the versatility of this protocol, which can readily be applied to a variety of different bone and mineralized tissues for their study in SEM. Comparing Fig. 5 to Fig. 4A/B), it is noted that similar imaging quality could be resolved in both high and low vacuum conditions, where both highlight the resolution of similar structural microfeatures of bone.

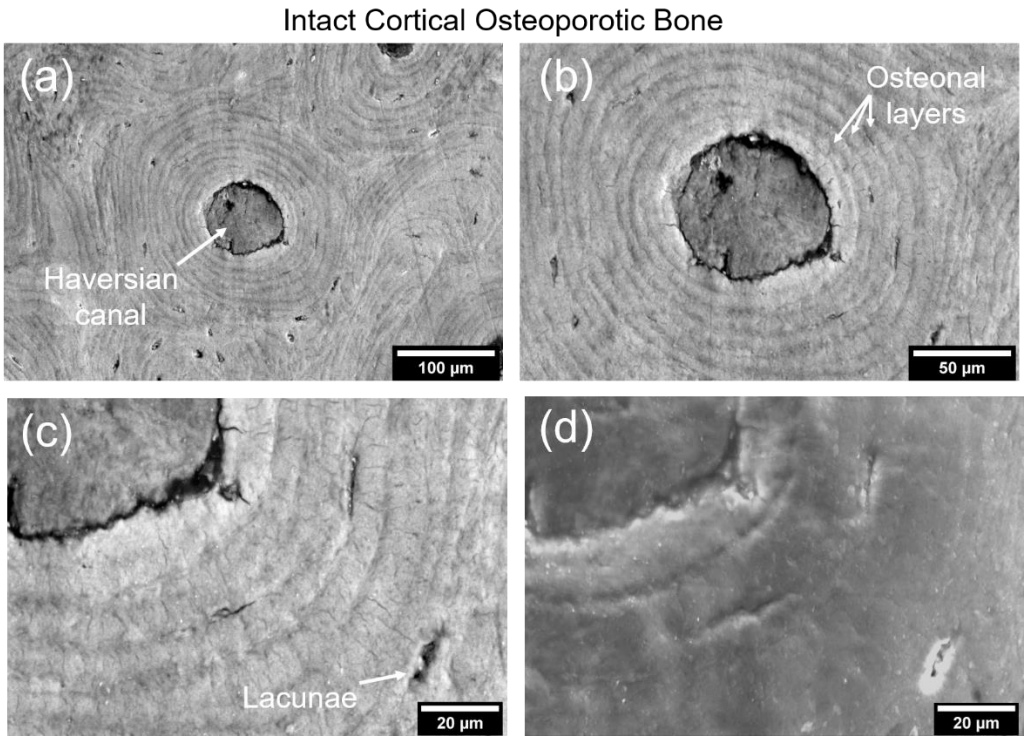

Figure 5. RTIL 10% v/v [BMI][BF_4] treated intact, unfractured osteoporotic cortical bone samples, showing in (a-c) BSE SEM images and (d) SE SEM of image of (c), all in high vacuum condition. Clear bone structural microfeatures can be distinguished such as a haversian canal at the center of (a,b) and circumferential osteonal layers can be distinguished, showing similar imaging quality in comparison to low vacuum observation in Fig. 4(a,b).

Figure 6 exemplifies the applications of RTILs in investigating highly topographical samples such as fracture surfaces to elucidate fracture mechanisms and modes of failure in nonconductive materials such as bone. For such bone segments, which may be over >1cm^3 in size, their preparation through conventional means is lengthy (highlighted by Fig. 1) and may influence the morphologies being observed (Kellenberger et al., 1992; Li et al., 2017; McKee et al., 1991; Utku et al., 2008). Here, the RTIL method presents a key method that can be used quickly and efficiently in lieu of conventional means to observe large fracture segments, without involving fixation and dehydration steps.

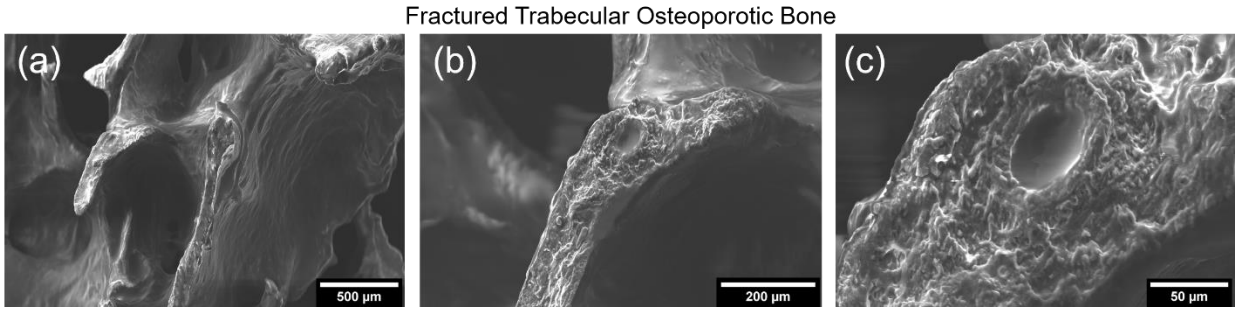

Figure 6. SE SEM images of RTIL 10% v/v [BMI][BF_4] treated fractured osteoporotic trabecular bone in high vacuum condition at successively higher magnification (a-c). Fine structural fracture surface and topography can be resolved with minimal charging effects.

3.4. Comparison to Dehydrated Bone

To evaluate the effectiveness of the optimal 10% v/v [BMI][BF_4] treatment against conventional methods, healthy bone specimens with cortical and trabecular segments were sectioned, dehydrated, and sputter-coated with gold. The samples were left unfixed to better compare to the unfixed RTIL treated samples. The conventionally prepared sample imaged in high vacuum BSE and SE mode is shown with both cortical and trabecular bone in Fig. 7.

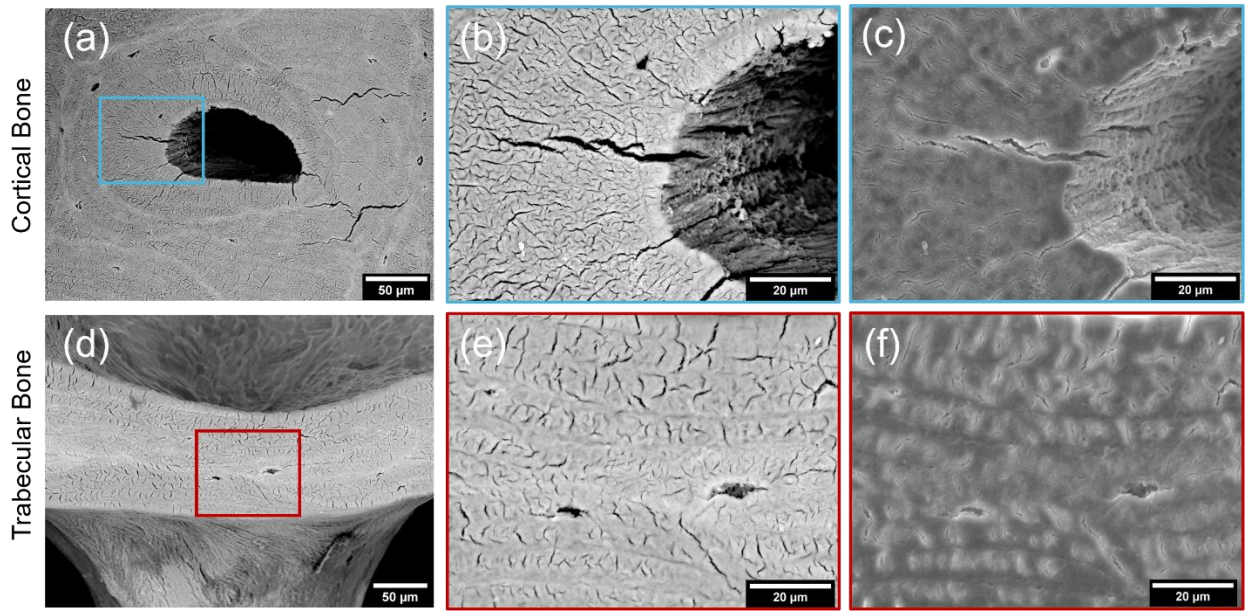

Figure 7. BSE SEM images of healthy dehydrated bone in high-vacuum conditions, highlighting both cortical bone (a,b) and trabecular bone (d,e), with SE SEM images featured in (c,f). Inset on (a) represents the edge of a lacunae and (d) inset highlights two lacunae. Similar to Fig. 4, fine structural details can be distinguished such as osteonal and lamellar bone as well as osteocyte lacunae; however, the structure has been significantly impacted by dehydration and microcracks are more prominent in comparison to the RTIL scheme, making them more susceptible to edge-effect charging in SE mode.

Distinct differences between the RTIL and conventionally treated samples can be noted. Microcracks are observed in greater number in the conventionally prepared dehydrated samples. While some cracks may be naturally occurring, it is suspected that most are artifacts from sample preparation methods. Microcracks are commonly a result of preparation methods such as polishing and dehydration steps (Shah et al., 2019). Given that all bone samples were ground and polished following the same procedure, it is suspected that most of these cracks are a direct result of dehydration, as minimal cracks are observed in Fig. 4 for the 10% v/v [BMI][BF_4] treated sample. This indicates that the RTIL application process may be used to effectively mitigate sample damage in high-resolution imaging, which may not be possible with conventional preparations that involve dehydration and harsh chemical fixation.

The additional microcracks made the structure more prominently affected by bright-edge charging effects not mitigated through gold coating. This effect arises from escaping surface electrons when imaged in SE modality (Seiler, 1983). In comparison, SE imaging from Fig. 5(d) with the 10% v/v [BMI][BF_4] treatment shows mitigation of this effect with minimal cracking. Similar RTIL treatments in SEM have been found to successfully mitigate edge-effect charging of biological samples with sharp edges and/or pointed features such as basidiospores and protists (Ishida et al., 2016; Yanaga et al., 2012).

3.5. RTIL Treatment and Elemental Analysis

Another essential utility of RTIL-based application methods is its potential to allow for EDS analysis on hydrated bone samples. Figure 8 demonstrates that EDS analysis can be applied to healthy bone in low-vacuum mode using the 10% v/v [BMI][BF_4] preparation as an example. An osteon is shown in the healthy bone in Fig. 8 (a), which was selected as a region of interest with known differences in bone mineral density for EDS analysis. Given that bone is a natural composite material composed primarily of calcium phosphate hydroxyapatite crystals, organic components, and unbound water, it was expected that C, Ca, P, and O would be key detectable elements in the structure and that higher density mineralized regions would have higher amounts of Ca and P (Clarke, 2008; Milovanovic et al., 2018; Shah et al., 2019; Skedros et al., 2005).

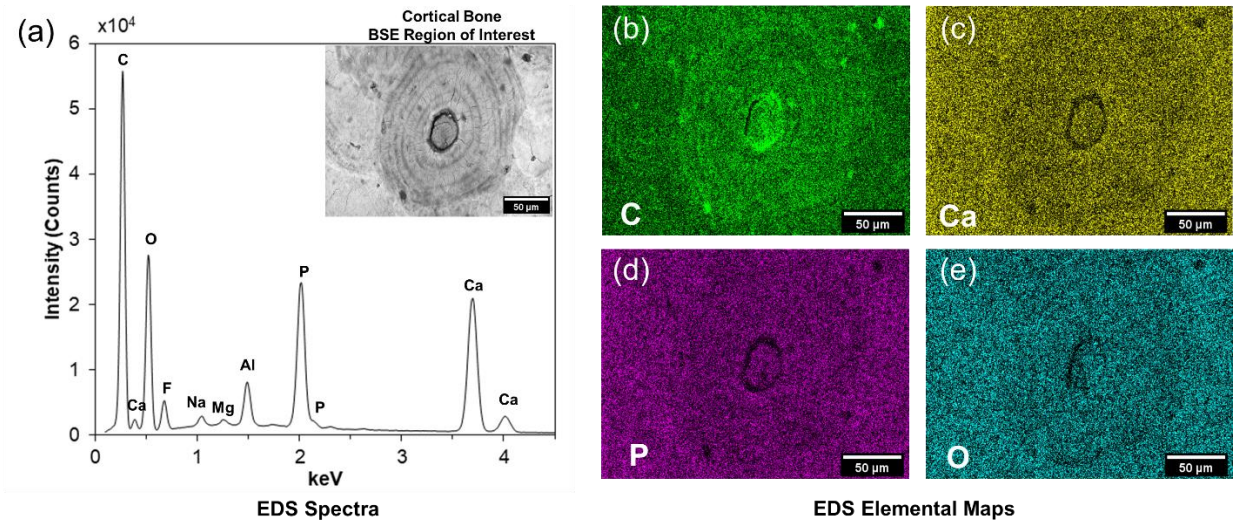

Figure 8. EDS analysis applied in imaging healthy cortical bone in low-vacuum mode using the 10% v/v [BMI][BF_4] (a) EDS spectra collected during analysis, with BSE image inset highlighting the cortical region of interest considered, where distinct peaks are noted for C, Ca, P, O, Na, F, and Mg; trace amounts of N, Si, Cl and S were also noted. Corresponding EDS elemental maps for characteristic elements present in bone structures (b) C, (c) Ca, (d) P, and (e) O, are shown.

A typical EDS spectrum collected during analysis is shown in Fig. 8 (a), where distinct peaks are noted for C, Ca, P, O, Na, F, and Mg; trace amounts of N, Si, Cl and S were also noted. Elemental detection of fluorine is attributed to the [BMI][BF_4] RTIL, where boron could have also been expected to be able to be detected though likely its peak was unable to be distinguished due to the strong nearby by carbon peak in the spectra. Figure 8 (b-e) depicts elemental mappings of the major constituents C, Ca, P, and O. Higher detection of Ca and P outside of the central osteon and a higher detection of C within this full osteon demonstrate the lower mineral to matrix composition, which is known to be associated with newly remodelled osteons compared to older or interstitial bone (Milovanovic et al., 2018; Skedros et al., 2005). This finding corroborates qualitative BSE imaging, Fig. 8 (a) (inset), which by its darker contrast indicates the central osteon has a lower mineral density.

It has been suggested reporting Ca:P ratios in lieu of wt% of each component as a reliable measure of composition in bone (Zaichick and Tzaphlidou, 2002). In this consideration for the region analyzed in Fig. 8 (a), a ratio of 1.9 Ca:P can be reported. This aligns well with median Ca:P values that were reported for cortical bone in the femoral neck summarized by Zaichick et al. (Zaichick and Tzaphlidou, 2002) and is slightly off from the expected 1.67 Ca:P ratio for stoichiometric hydroxyapatite.

Several effects could influence the results obtained from EDS analysis, such as noise in the spectra from detection and SEM imaging conditions as well as the RTIL treatment itself. Abe et al. noted in their work that higher accumulated regions of the RTIL treatment can lead to a lack of penetration of the electron beam to a region of interest and lead to a lack of signal detection, where they used a 5kV electron beam (Abe et al., 2012). This effect can be mitigated by using a higher kV beam to get higher penetration within the sample and an optimal RTIL treatment that reduces RTIL pooling, as done in our work here with a 15kV beam and the optimal 10% v/v [BMI][BF_4] treatment. However, the underlying effect of the RTIL on the surface remains a presence in the spectra, as exemplified by the strong F peak in Fig. 8 (a), which is not normally present in bone in such amount. One advantage to such an RTIL treatment is the F peak present does not have an overlapping peak with P, which both common Pt and Au coatings for bone can have with their M level characteristic X-rays peaks (Goldstein et al., 2018). This can lead to challenges in the interpretation of concentration of P in characterization and its detection more challenging in conventional preparation schemes using Pt or Au sputter coatings.

3.6. Potential Pitfalls and Challenges

Despite the quick turn-around time for preparing samples with RTILs, the treatment is temporary. After 6-7 days, RTIL-treated SEM samples can begin to show signs of debris accumulation, carbon deposition, and charging effects (Ishigaki et al., 2011b, 2011c; Lee et al., 2021). Samples may also begin to degrade or foul, depending on the sample. This is a clear disadvantage of RTIL-based SEM compared to conventional methods, which typically include a fixation step to prevent sample degradation; however, the scheme may still be applied to fixed samples which could help preserve their structure for longer. Careful storage in a closed system such as a desiccator has been shown to mitigate these contamination effects up to one month, after which the RTIL treatment must be reapplied (Ishigaki et al., 2011a). Limited work explores the effectiveness of re-applying RTILs to further treat samples, however, which raises caution for its reapplication considering the effects of consecutive RTIL treatment on sample structure and quality.

A possible concern with using [EMI][BF_4] and [BMI][BF_4] RTILs is the formation of HF by-products through potential degradation mechanisms involving aqueous $[BF4]^-$, particularly at elevated temperatures (Freire et al., 2010; Radosavljević et al., 1979). Tsuda et al. (Tsuda et al., 2014) theorized that using [EMI][BF_4] and [BMI][BF_4] in aqueous solution for SEM treatment led to the formation of HF, which they discussed may have decreased the size of superabsorbent polymer particles observed in their work, as well as drastically changed their particle surface morphologies. In the work presented here, we noted no signs of degradation in the bone samples studied during SEM imaging. Due to the high affinity of HF towards calcium, which typically attacks bone structures and leads to calcium depletion (Bertolini, 1992), it would be expected that noticeable degradation may have occurred if significant amounts of HF had formed. Thus, the risk of HF-related damage is believed to be negligible under the imaging conditions and RTIL concentrations used in this study.

The success of this RTIL-based imaging protocol has permitted the efficient observation of hydrated bone samples, in the absence of any specialized equipment or complicated preparation steps. The work poses several implications to the bone imaging community – exploring new preparation methods to observe hydrated natural tissues quickly and efficiently. This work offers attractive alternatives for studying the hierarchical structure of bone and other mineralized tissues, providing a new method to perform correlative observations of their features. Current methodologies require steps that may inadvertently compromise the natural structure of bone tissue, namely dehydration and fixation (Kellenberger et al., 1992; Li et al., 2017; McKee et al., 1991; Utku et al., 2008). This calls into question the validity and reliability of data collected using these methods.

The other state-of-the-art approach for retaining bone structure during imaging is cryo-preservation (Kerschnitzki et al., 2016; Mahamid et al., 2011, 2010). This methodology preserves the hydrated structure of bone, mitigating issues described that arise from conventional preparation involving dehydration. Moreover, cryo-EM methods can produce clearer images due to the limited amount of electron scatter in vitrified liquids in comparison to liquids in their native state (Patterson et al., 2017). However, once vitrified, similar densities of soft materials and the vitrified mediums can reduce Z-contrast in imaging and lower the signal-to-noise ratio (He et al., 2019). However, the cryo-EM vitrification process and sample preparation require extensive experience and a relatively expensive suite of equipment to achieve impeccable results in comparison to the simply applied RTIL method presented in this work.

In summary, we demonstrate that RTIL treatment presents a feasible method to study the hierarchical structure of bone. While there exists apprehension to the application of such liquid-based SEM preparation techniques (DiCecco et al., 2021), our present work, and the plethora of other works on biological materials (Golding et al., 2016; Komai et al., 2014; Kuwabata et al., 2006; Lee et al., 2021; Lu et al., 2019; Tsuda et al., 2011), gives further confidence to this technique.

4. Conclusions

This work highlights a new methodology to study bone in its natural, hydrated state through SEM imaging using an RTIL-based treatment method. The optimization of this treatment was explored using [EMI][BF_4] and [BMI][BF_4] RTILs at 5, 10, and 25% v/v in aqueous solution at varying imaging conditions. The described protocol is simple, efficient, and can be quickly applied to fresh bone samples as an alternative SEM preparation method to lengthy and

laborious conventional means. Moreover, the RTIL treatment is suggested to better preserve natural bone structure, resulting in minimal cracking as observed in comparison to traditional preparation schemes involving dehydration. An optimal treatment identified in this work involved a 60-second application method with 10% v/v [BMI][BF_4] treatment for hydrated, unfixed bone. The described protocol was used to observe polished and fractured surfaces of bone in both high and low vacuum mode SEM, with acceleration voltages of 15 kV, and in both SE and BSE imaging modes. Minimal charging effects were observed using this treatment and we showed that it was still possible to perform elemental analysis, such as EDS, on RTIL-treated bone. This proof-of-concept work highlights the versatility and feasibility of this technique for observing a variety of healthy and pathological mineralized bone samples for wide-ranging applications. This work lays the foundation for the biological community to continue to explore RTIL-based techniques in the study of natural and hydrated tissues.

Acknowledgements

Financial support provided by the Natural Sciences and Engineering Research Council of Canada (NSERC) Discovery Grant program (RGPIN-2020-05722), Canada Research Chairs program (LS and KG), the Vanier Canada Graduate Scholarship (Vanier CGS, L-AD) program and McMaster Engineering Big Ideas Grant is greatly acknowledged. Electron microscopy was performed at the Canadian Centre for Electron Microscopy (also supported by NSERC and other government agencies). Illustrations in this work highlighting the process pathways were created with BioRender.com.

Conflicts of Interest

The authors declare no conflict of interest.

Data Availability

Data is available upon request to the corresponding author.

References

Abe, S., Hyono, A., Machida, Y., Watari, F., Yonezawa, T., 2012. Conductivity Preparation by Choline Lactate Ethanol Solution for SEM Observation: Both Hard and Soft Tissues in Living Matter. Nano Biomed 4, 18–23. https://doi.org/10.11344/nano.4.18

Arimoto, S., Sugimura, M., Kageyama, H., Torimoto, T., Kuwabata, S., 2008. Development of new techniques for scanning electron microscope observation using ionic liquid. Electrochim Acta 53, 6228–6234. https://doi.org/10.1016/j.electacta.2008.01.001

Bertolini, J.C., 1992. Hydrofluoric acid: A review of toxicity. J Emerg Medicine 10, 163–168. https://doi.org/10.1016/0736-4679(92)90211-b

Binkley, D.M., Deering, J., Yuan, H., Gourrier, A., Grandfield, K., 2020. Ellipsoidal mesoscale mineralization pattern in human cortical bone revealed in 3D by plasma focused ion beam serial sectioning. J Struct Biol 107615. https://doi.org/10.1016/j.jsb.2020.107615

Binkley, D.M., Grandfield, K., 2017. Advances in Multiscale Characterization Techniques of Bone and Biomaterials Interfaces. Acs Biomater Sci Eng 4, 3678–3690. https://doi.org/10.1021/acsbiomaterials.7b00420

Boyde, A., Jones, S.J., 1996. Scanning electron microscopy of bone: Instrument, specimen, and issues. Microsc Res Techniq 33, 92–120. https://doi.org/10.1002/(sici)1097-0029(19960201)33:2<92::aid-jemt2>3.0.co;2-0

Boyde, A., Maconnachie, E., Reid, S.A., Delling, G., Mundy, G.R., 1986. Scanning electron microscopy in bone pathology: review of methods, potential and applications. Scanning Microscopy 1537–54.

Braidotti, P., Bemporad, E., D'Alessio, T., Sciuto, S.A., Stagni, L., 2000. Tensile experiments and SEM fractography on bovine subchondral bone. J Biomech 33, 1153–1157. https://doi.org/10.1016/s0021-9290(00)00074-9

Chissoe, W.F., Vezey, E.L., Skvarla, J.J., 1995. The Use of Osmium-Thiocarbohydrazide for Structural Stabilization and Enhancement of Secondary Electron Images in Scanning Electron Microscopy of Pollen. Grana 34, 317–324. https://doi.org/10.1080/00173139509429065

Clarke, B., 2008. Normal Bone Anatomy and Physiology. Clin J Am Soc Nephro 3, S131–S139. https://doi.org/10.2215/cjn.04151206

Dempster, D.W., Shane, E., Horbert, W., Lindsay, R., 1986. A simple method for correlative light and scanning electron microscopy of human iliac crest bone biopsies: Qualitative observations in normal and osteoporotic subjects. J Bone Miner Res 1, 15–21. https://doi.org/10.1002/jbmr.5650010105

DiCecco, L.-A., D'Elia, A., Miller, C., Sask, K.N., Soleymani, L., Grandfield, K., 2021. Electron Microscopy Imaging Applications of Room Temperature Ionic Liquids in the Biological Field – A Review. Chembiochem. https://doi.org/10.1002/cbic.202100041

Freire, M.G., Neves, C.M.S.S., Marrucho, I.M., Coutinho, J.A.P., Fernandes, A.M., 2010. Hydrolysis of Tetrafluoroborate and Hexafluorophosphate Counter Ions in Imidazolium-Based Ionic Liquids †. J Phys Chem 114, 3744–3749. https://doi.org/10.1021/jp903292n

Golding, C.G., Lamboo, L.L., Beniac, D.R., Booth, T.F., 2016. The scanning electron microscope in microbiology and diagnosis of infectious disease. Sci Rep-uk 6, 26516. https://doi.org/10.1038/srep26516

Goldstein, J.I., Newbury, D.E., Michael, J.R., Ritchie, N.W.M., Scott, J.H.J., Joy, D.C., 2018. Scanning Electron Microscopy and X-Ray Microanalysis. Springer, New York NY.

Hagiwara, R., Ito, Y., 2000. Room temperature ionic liquids of alkylimidazolium cations and fluoroanions. J Fluorine Chem 105, 221–227. https://doi.org/10.1016/s0022-1139(99)00267-5

He, K., Shokuhfar, T., Shahbazian-Yassar, R., 2019. Imaging of soft materials using in situ liquid-cell transmission electron microscopy. J Phys Condens Matter 31, 103001. https://doi.org/10.1088/1361-648x/aaf616

Hiller, L.P., Stover, S.M., Gibson, V.A., Gibeling, J.C., Prater, C.S., Hazelwood, S.J., Yeh, O.C., Martin, R.B., 2003. Osteon pullout in the equine third metacarpal bone: Effects of ex vivo fatigue. J Orthopaed Res 21, 481–488. https://doi.org/10.1016/s0736-0266(02)00232-2

Ishida, H., Gobara, Y., Kobayashi, M., Suzaki, T., 2016. Use of Ionic Liquid for Scanning Electron Microscopy of Protists. International Journal of New Technology and Research 2, 43–46.

Ishigaki, Y., Nakamura, Y., Takehara, T., Kurihara, T., Koga, H., Takegami, T., Nakagawa, H., Nemoto, N., Tomosugi, N., Kuwabata, S., Miyazawa, S., 2011a. Comparative study of hydrophilic and hydrophobic ionic liquids for observing cultured human cells by scanning electron microscopy. Microsc Res Techniq 74, 1104–1108. https://doi.org/10.1002/jemt.21001

Ishigaki, Y., Nakamura, Y., Takehara, T., Nemoto, N., Kurihara, T., Koga, H., Nakagawa, H., Takegami, T., Tomosugi, N., Miyazawa, S., Kuwabata, S., 2011b. Ionic liquid enables simple and rapid sample preparation of human culturing cells for scanning electron microscope analysis. Microsc Res Techniq 74, 415–420. https://doi.org/10.1002/jemt.20924

Ishigaki, Y., Nakamura, Y., Takehara, T., Shimasaki, T., Tatsuno, T., Takano, F., Ueda, Y., Motoo, Y., Takegami, T., Nakagawa, H., Kuwabata, S., Nemoto, N., Tomosugi, N., Miyazawa, S., 2011c. Scanning electron microscopy with an ionic liquid reveals the loss of mitotic protrusions of cells during the epithelial–mesenchymal transition. Microsc Res Techniq 74, 1024–1031. https://doi.org/10.1002/jemt.20989

Jazinizadeh, F., Mohammadi, H., Quenneville, C.E., 2020. Comparing the fracture limits of the proximal femur under impact and quasi-static conditions in simulation of a sideways fall. J Mech Behav Biomed 103, 103593. https://doi.org/10.1016/j.jmbbm.2019.103593

Kanbayashi, T., Miyafuji, H., 2016. Microscopic characterization of tension wood cell walls of Japanese beech (Fagus crenata) treated with ionic liquids. Micron 88, 24–29. https://doi.org/10.1016/j.micron.2016.05.007

Kellenberger, E., Johansen, R., Maeder, M., Bohrmann, B., Stauffer, E., Villiger, W., 1992. Artefacts and morphological changes during chemical fixation. J Microsc-oxford 168, 181–201. https://doi.org/10.1111/j.1365-2818.1992.tb03260.x

Kerschnitzki, M., Akiva, A., Shoham, A.B., Asscher, Y., Wagermaier, W., Fratzl, P., Addadi, L., Weiner, S., 2016. Bone mineralization pathways during the rapid growth of embryonic chicken long bones. J Struct Biol 195, 82–92. https://doi.org/10.1016/j.jsb.2016.04.011

Kini, U., Nandeesh, B.N., 2012. Physiology of Bone Formation, Remodeling, and Metabolism, in: Fogelman, I., Gnanasegaran, G., Wall, H. van der (Eds.), Radionuclide and Hybrid Bone Imaging. Springer-Verlag Berlin Heidelberg, pp. 29–57. https://doi.org/10.1007/978-3-642-02400-9_2

Komai, F., Okada, K., Inoue, Y., Yada, M., Tanaka, O., Kuwabata, S., 2014. SEM Observation of Wet Lily Pollen Grains Pretreated with Ionic Liquid. J Jpn Soc Hortic Sci 83, 317–321. https://doi.org/10.2503/jjshs1.mi-008

Kuwabata, S., Kongkanand, A., Oyamatsu, D., Torimoto, T., 2006. Observation of Ionic Liquid by Scanning Electron Microscope. Chem Lett 35, 600–601. https://doi.org/10.1246/cl.2006.600

Lee, B.E.J., DiCecco, L.-A., Exir, H., Weck, A., Sask, K.N., Grandfield, K., 2021. Simultaneous Visualization of Wet Cells and Nanostructured Biomaterials in SEM using Ionic Liquids. ChemBioChem 22, 571–576. https://doi.org/10.1002/cbic.202000552

Li, Y., Almassalha, L.M., Chandler, J.E., Zhou, X., Stypula-Cyrus, Y.E., Hujsak, K.A., Roth, E.W., Bleher, R., Subramanian, H., Szleifer, I., Dravid, V.P., Backman, V., 2017. The effects of chemical fixation on the cellular nanostructure. Exp Cell Res 358, 253–259. https://doi.org/10.1016/j.yexcr.2017.06.022

Lu, B.-J., Li, J.-R., Tai, H.-C., Cai, W., Tseng, H.-H., Hsieh, Y.-T., 2019. A facile ionic-liquid pretreatment method for the examination of archaeological wood by scanning electron microscopy. Sci Rep-uk 9, 13253. https://doi.org/10.1038/s41598-019-49773-y

Mahamid, J., Aichmayer, B., Shimoni, E., Ziblat, R., Li, C., Siegel, S., Paris, O., Fratzl, P., Weiner, S., Addadi, L., 2010. Mapping amorphous calcium phosphate transformation into crystalline mineral from the cell to the bone in zebrafish fin rays. Proc National Acad Sci 107, 6316–6321. https://doi.org/10.1073/pnas.0914218107

Mahamid, J., Sharir, A., Gur, D., Zelzer, E., Addadi, L., Weiner, S., 2011. Bone mineralization proceeds through intracellular calcium phosphate loaded vesicles: A cryo-electron microscopy study. J Struct Biol 174, 527–535. https://doi.org/10.1016/j.jsb.2011.03.014

McKee, M.D., Nanci, A., Landis, W.J., Gotoh, Y., Gerstenfeld, L.C., Glimcher, M.J., 1991. Effects of fixation and demineralization on the retention of bone phosphoprotein and other matrix components as evaluated by

biochemical analyses and quantitative immunocytochemistry. J Bone Miner Res 6, 937–945. https://doi.org/10.1002/jbmr.5650060907

Milovanovic, P., Scheidt, A. vom, Mletzko, K., Sarau, G., Püschel, K., Djuric, M., Amling, M., Christiansen, S., Busse, B., 2018. Bone tissue aging affects mineralization of cement lines. Bone 110, 187–193. https://doi.org/10.1016/j.bone.2018.02.004

Patterson, J.P., Xu, Y., Moradi, M.-A., Sommerdijk, N.A.J.M., Friedrich, H., 2017. CryoTEM as an Advanced Analytical Tool for Materials Chemists. Accounts Chem Res 50, 1495–1501. https://doi.org/10.1021/acs.accounts.7b00107

Radosavljević, S., Ŝćepanović, V., Stević, S., Milojković, D., 1979. Effect of boric acid on tetrafluoroborate ion hydrolysis in solutions of tetrafluoroboric acid. J Fluorine Chem 13, 465–471. https://doi.org/10.1016/s0022-1139(00)83094-8

Reznikov, N., Almany-Magal, R., Shahar, R., Weiner, S., 2013. Three-dimensional imaging of collagen fibril organization in rat circumferential lamellar bone using a dual beam electron microscope reveals ordered and disordered sub-lamellar structures. Bone 52, 676–683. https://doi.org/10.1016/j.bone.2012.10.034

Roschger, P., Fratzl, P., Eschberger, J., Klaushofer, K., 1998. Validation of quantitative backscattered electron imaging for the measurement of mineral density distribution in human bone biopsies. Bone 23, 319–326. https://doi.org/10.1016/s8756-3282(98)00112-4

Seiler, H., 1983. Secondary electron emission in the scanning electron microscope. J Appl Phys 54, R1–R18. https://doi.org/10.1063/1.332840

Shah, F.A., Ruscsák, K., Palmquist, A., 2019. 50 years of scanning electron microscopy of bone—a comprehensive overview of the important discoveries made and insights gained into bone material properties in health, disease, and taphonomy. Bone Res 7, 15. https://doi.org/10.1038/s41413-019-0053-z

Shah, F.A., Snis, A., Matic, A., Thomsen, P., Palmquist, A., 2016. 3D printed Ti6Al4V implant surface promotes bone maturation and retains a higher density of less aged osteocytes at the bone-implant interface. Acta Biomater 30, 357–367. https://doi.org/10.1016/j.actbio.2015.11.013

Skedros, J.G., Holmes, J.L., Vajda, E.G., Bloebaum, R.D., 2005. Cement lines of secondary osteons in human bone are not mineral-deficient: New data in a historical perspective. Anatomical Rec Part Discov Mol Cell Evol Biology 286A, 781–803. https://doi.org/10.1002/ar.a.20214

Tedesco, J., Lee, B.E.J., Lin, A.Y.W., Binkley, D.M., Delaney, K.H., Kwiecien, J.M., Grandfield, K., 2017. Osseointegration of a 3D Printed Stemmed Titanium Dental Implant: A Pilot Study. Int J Dent 2017, 1–11. https://doi.org/10.1155/2017/5920714

Tsuda, T., Kuwabata, S., 2020. Electron microscopy using ionic liquids for life and materials sciences. Microscopy 69, 183–195. https://doi.org/10.1093/jmicro/dfaa013

Tsuda, T., Mochizuki, E., Kishida, S., Iwasaki, K., Tsunashima, K., Kuwabata, S., 2014. SEM Observation of Hydrous Superabsorbent Polymer Pretreated with Room-Temperature Ionic Liquids. Plos One 9, e91193. https://doi.org/10.1371/journal.pone.0091193

Tsuda, T., Nemoto, N., Kawakami, K., Mochizuki, E., Kishida, S., Tajiri, T., Kushibiki, T., Kuwabata, S., 2011. SEM Observation of Wet Biological Specimens Pretreated with Room-Temperature Ionic Liquid. Chembiochem 12, 2547–2550. https://doi.org/10.1002/cbic.201100476

Utku, F.S., Klein, E., Saybasili, H., Yucesoy, C.A., Weiner, S., 2008. Probing the role of water in lamellar bone by dehydration in the environmental scanning electron microscope. J Struct Biol 162, 361–367. https://doi.org/10.1016/j.jsb.2008.01.004

Welton, T., 1999. Room-Temperature Ionic Liquids. Solvents for Synthesis and Catalysis. Chem Rev 99, 2071–2084. https://doi.org/10.1021/cr980032t

Yanaga, K., Maekawa, N., Shimomura, N., Ishigaki, Y., Nakamura, Y., Takegami, T., Tomosugi, N., Miyazawa, S., Kuwabata, S., 2012. Use of ionic liquid in fungal taxonomic study of ultrastructure of basidiospore ornamentation. Mycol Prog 11, 343–347. https://doi.org/10.1007/s11557-011-0794-6

Zaichick, V., Tzaphlidou, M., 2002. Determination of calcium, phosphorus, and the calcium/phosphorus ratio in cortical bone from the human femoral neck by neutron activation analysis. Appl Radiat Isotopes 56, 781–786. https://doi.org/10.1016/s0969-8043(02)00066-0

Figure Captions

Figure 1. Illustration of conventional SEM preparation methods used for bone with time of each step approximated (estimation for bone specimens 1 cm^3 or larger). Note that staining and embedding procedures would further lengthen the preparation time.

Figure 2. Schematic illustrating the specific RTIL treatment process used in this work for SEM imaging of hydrated, unfixed bone samples.

Figure 3. BSE SEM images of healthy bone taken in low-vacuum conditions. Samples were treated with 5, 10, or 25% v/v of [BMI][BF_4] (a-c) or [EMI][BF_4] (d-f) in water for 60 s. All images show osteons in a central location of each image surrounded by concentric lamellae bone centralized around a harversian canal. At higher concentrations of 25% v/v, fine details in the bone structure were obscured while liquid pooling was also observed on the structure. The 10% v/v had limited issues with charging and could be used readily for high resolution in both low and high-vacuum conditions, thus performed optimally within the treatments explored.

Figure 4. BSE SEM images of healthy bone in low-vacuum conditions treated with 10% v/v [BMI][BF4]. Both cortical bone (a,b) with visible harversian canals and trabecular bone (c,d) were easily imaged with this concentration. At higher magnification (b,d) both osteonal and lamellar bone as well as lacunae where osteocytes are located are visible. Minimal cracks are observed.

Figure 5. RTIL 10% v/v [BMI][BF_4] treated intact, unfractured osteoporotic cortical bone samples, showing in (a-c) BSE SEM images and (d) SE SEM of image of (c), all in high vacuum condition. Clear bone structural microfeatures can be distinguished such as a haversian canal at the center of (a,b) and circumferential osteonal layers can be distinguished, showing similar imaging quality in comparison to low vacuum observation in Fig. 4(a,b).

Figure 6. SE SEM images of RTIL 10% v/v [BMI][BF_4] treated fractured osteoporotic trabecular bone in high vacuum condition at successively higher magnification (a-c). Fine structural fracture surface and topography can be resolved with minimal charging effects.

Figure 7. BSE SEM images of healthy dehydrated bone in high-vacuum conditions, highlighting both cortical bone (a,b) and trabecular bone (d,e), with SE SEM images featured in (c,f). Inset on (a) represents the edge of a lacunae and (d) inset highlights two lacunae. Similar to Fig. 4, fine structural details can be distinguished such as osteonal and lamellar bone as well as osteocyte lacunae; however, the structure has been significantly impacted by dehydration and microcracks are more prominent in comparison to the RTIL scheme, making them more susceptible to edge-effect charging in SE mode.

Figure 8. EDS analysis applied in imaging healthy cortical bone in low-vacuum mode using the 10% v/v [BMI][BF_4] (a) EDS spectra collected during analysis, with BSE image inset highlighting the cortical region of interest considered, where distinct peaks are noted for C, Ca, P, O, Na, F, and Mg; trace amounts of N, Si, Cl and S were also noted. Corresponding EDS elemental maps for characteristic elements present in bone structures (b) C, (c) Ca, (d) P, and (e) O, are shown.

Author Contributions

Conceptualization: Liza-Anastasia DiCecco, Kathryn Grandfield
Methodology: Liza-Anastasia DiCecco, Andrew D'Elia
Data curation: Liza-Anastasia DiCecco
Formal analysis: Liza-Anastasia DiCecco, Andrew D'Elia
Funding acquisitions and supervision: Kathryn Grandfield, Leyla Soleymani, Cheryl Quenneville
Writing- first draft: Liza-Anastasia DiCecco
Review and editing: Liza-Anastasia DiCecco, Andrew D'Elia, Leyla Soleymani, Cheryl Quenneville, Kathryn Grandfield